nature nanotechnology

SUPPLEMENTARY INFORMATION

DOI: 10.1038/NNANO.2011.88

Supporting Information

Single-molecule transport across an individual biomimetic nuclear pore complex

Stefan W. Kowalczyk, Larisa Kapinos, Timothy R. Blosser, Tomás Magalhães, Pauline van Nies, Roderick Y. H. Lim, and Cees Dekker

Overview of the Supporting Information:

1. Schematic of the chemistry used for Nup binding

2. Protein gels

3. Estimate of the Nup density in the pore

4. Charges and isoelectric points of BSA, Impβ, Nup98, and Nup153

5. Voltage (non-)dependence for Impβ translocations through a Nup-coated pore

6. Noise in bare and coated pores

7. Alternative exclusion structures

8. Example events of Impβ translocations through a Nup153-modified pore

9. Analysis of re-entry events of Impβ

10. Overview of measured event amplitudes, translocation times, and event rates

11. Dwell time histograms on linear scale

12. Event frequency versus voltage

13. Nanopore array

14. TIRF measurements

15. SPR measurements

16. Conformational characteristics of Nup98 and Nup153

© 2011 Macmillan Publishers Limited. All rights reserved.

1. Schematic of the chemistry used for Nup-binding

The chemistry used to attach the Nups to the surface consists of three steps. Figure S1 shows a schematic. We first coat the pores with APTES, leaving amine groups exposed (step 1 in Fig.S1). Next, we covalently bind the amines to cross linker Sulfo-SMCC leaving the surface terminated with thiol-reactive maleimides (step 2). We then bind the C-terminal FG-domains of the Nups (98 or 153) via terminal thiols (step 3).

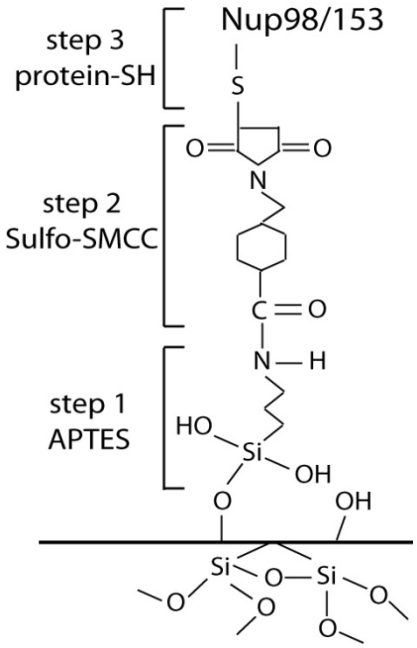

Figure S1. Schematic of the chemistry used to covalently bind Nups to the nanopore.

© 2011 Macmillan Publishers Limited. All rights reserved.

2. Protein gels

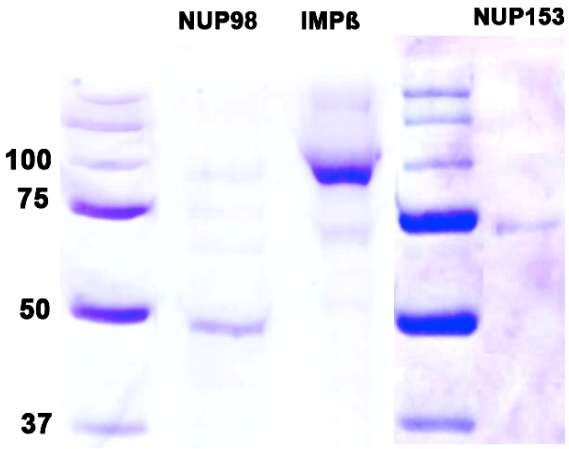

Figure S2. Commassie Brilliant Blue-stained SDS-PAGE (12% acrylamide) of Impβ (97 kDa), Nup98 (50 kDa) and Nup153 (62 kDa).

3. Estimate of the Nup density in the pore

The Nup density in the pore can be estimated as follows: We translocate Nups through a bare pore and quantify the reduction of conductance caused by its presence in the pore. We find that a single translocating Nup98 molecule reduces the open-pore conductance by 0.92 nS (see Fig.S3). This means that a typical pore of 40 nm in diameter, where the conductance reduces from 58 nS to 16 nS upon coating with Nup98, contains approximately 46 Nups. Given that the surface area of the pore is $2*\pi*20*20 \approx 2500$ nm^2, this means that the Nup density is of the order of 1 Nup per 54 nm^2 at the pore wall surface, i.e., each Nup occupies an area of ~ 7x7 nm^2. Given the hydrodynamic diameter of these proteins (~ 11 nm, as measured from dynamic light scattering (unpublished data); similar values for other Nups were reported in Ref. 1), this is a very high density.

© 2011 Macmillan Publishers Limited. All rights reserved.

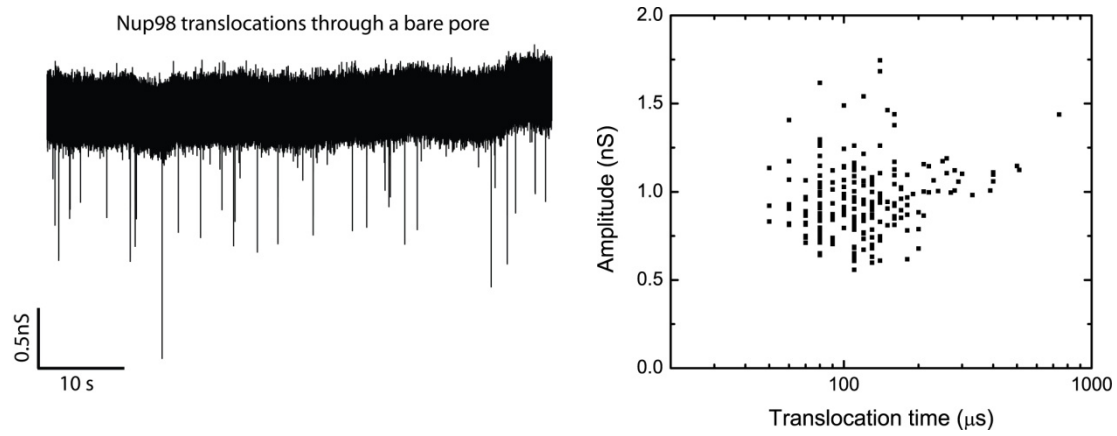

Figure S3. Nup98 translocation through a bare pore. (left) Example trace after addition of Nup98 in a bare pore. Downward spikes appear in the current trace upon addition of Nup98. Each spike is a single-molecule event. (right) Scatter diagram for Nup98 translocations. We find that one Nup molecule reduces the open-pore conductance by 0.92 ± 0.18 nS. The average dwell time is 107 ± 30 μs.

4. Charge and isoelectric points of BSA, Impβ, Nup98, and Nup153

The theoretical pIs (based on using their amino acid composition) of BSA and Impβ are slightly different (5.6-5.8 and 4.7, respectively, see Table T1). However, both values are clearly below pH=8, which will yield the same sign for both proteins in our experimental conditions. Furthermore, the experimental pIs of native (folded) BSA and Impβ can be different from the theoretical estimates, and indeed they are. For BSA, isoelectric focusing experiments give values of pI=4.6-4.9[2]. For Impβ such measurements had not been performed yet, and hence we performed such measurements ourselves, and found an experimental pI of 5.3 for the native (folded) Impβ (data shown in Fig.S4). We thus find that the experimental values for BSA range from 4.6 to 4.9 versus 5.3 for Impβ, which is not a great difference. Table T1 lists the charges of these two proteins. These values are not very different for BSA and Impβ. The size of both proteins is somewhat different. In fact, this further enhances our observations: based on size, the observation of a much lower permeability of BSA through the Nup-coated pores versus Impβ (which is bigger) makes this control only stronger.

© 2011 Macmillan Publishers Limited. All rights reserved.

Protein (total aa)	pI		# of neg. aa	# of pos. aa	Net charge at pH=7	Stokes diameter, nm (d_h)
	Theor. pI	Measured pI, IEF				
BSA (607 aa)	5.6-5.8	4.6-4.9[2]	99	86	13 -	7.4
Impβ (876 aa)	4.68	5.3	124	75	49 -	12
Nup98 (498 aa)	8.89		12	16	4 +	11.2
Nup153 (602 aa)	8.85		37	43	6 +	11.3

Table T1. Theoretical pI values and charges of various proteins (based on its sequence) and experimentally deduced pI values of the native (folded) protein as measured by isoelectric focusing.

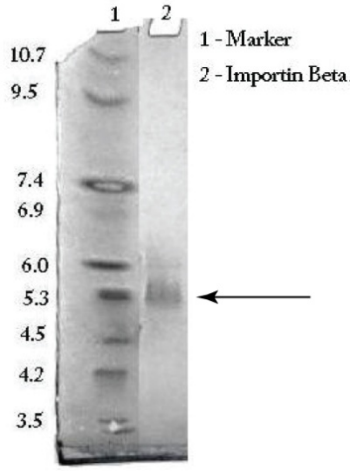

Figure S4. Isoelectric focusing gel, showing a pI of about 5.3 for native (folded) Impβ. The 5% polyacrylamide isoelectic gel (Novex IEF Gel from Invitrogen) consist of high-purity acrylamide, bisacrylamide, TEMED, APS, ultrapure water, and 2% ampholytes. It does not contain denaturing reagents.

5. Voltage (non-)dependence for Impβ translocations through a Nup-coated pore

As mentioned in the manuscript, the fact that we measure linear I-V relations (Fig.1d) up to an applied voltage of at least 200 mV indicates that the Nups in the nanopore are not significantly influenced by the applied electric field. We measured the voltage dependence of translocation times and amplitudes for Impβ translocation through a 35 nm diameter Nup-coated pore. Event amplitudes for Impβ translocations are found to be constant as a function of voltage (Fig.S5a), similar to the observations for bare pores. However, the behavior of translocation time versus voltage is different between bare and Nup-coated pores. The translocation times for bare pores scale inversely proportional

© 2011 Macmillan Publishers Limited. All rights reserved.

with voltage, $\tau \sim 1/V$ (see for example Ref. 36 in the main text), which appears *not* to be the case for Nup-coated pores. As presented in Fig.S5b, the dwell times for Impβ through a Nup-98 coated pore are constant within experimental error in the range probed (25-175 mV).

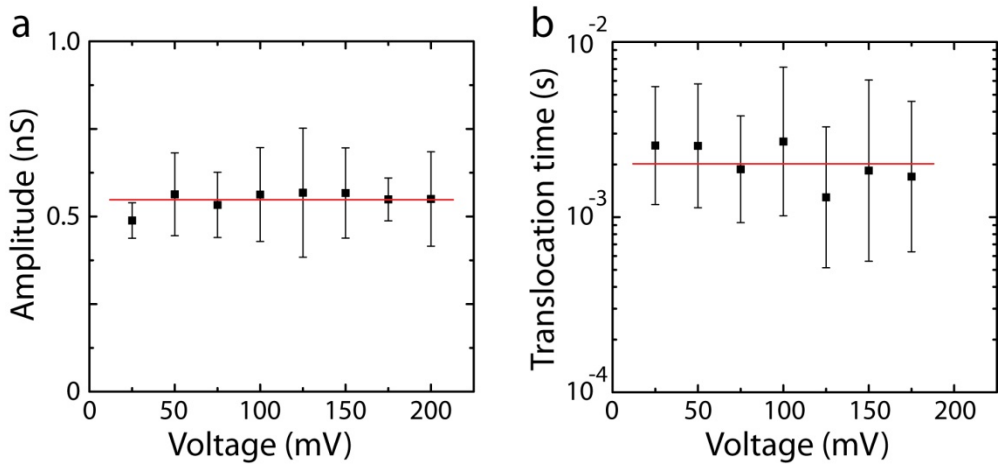

Figure S5. Voltage dependence of translocation time and amplitude for Impβ translocations through a Nup98-coated pore. We observe no dependence of translocation time and amplitude on voltage.

This is strong evidence showing that the dominant effect determining the translocation time is not set by the applied voltage, but by the interaction of the Impβ with the FG-domain Nups. We find values of 0.55 ± 0.01 nS for the amplitudes, and 2.0 ± 0.2 ms for the translocation times over the entire range of voltages probed here, where the error bars denote the standard deviation due to the variation of points. Note that the error bars in Fig.S5 indicate the width of the Gaussian fits to the data at each voltage.

6. Noise in bare and coated pores

A direct probe to study the properties of a nanopore is to examine its ionic current signature. In addition to the average current, the noise characteristics can provide nanoscopic information about the state of a nanopore. As mentioned in the manuscript, we see an increase in low-frequency noise upon coating of a nanopore with Nups, as presented in Fig.S6. Importantly, the additional noise for the Nup-coated pores does not significantly decrease the signal-to-noise ratio in our single-molecule translocation

© 2011 Macmillan Publishers Limited. All rights reserved.

measurements because typical transport events occur in the millisecond range (indicated in green in Fig.S6), where the noise level is similar to that of bare pores.

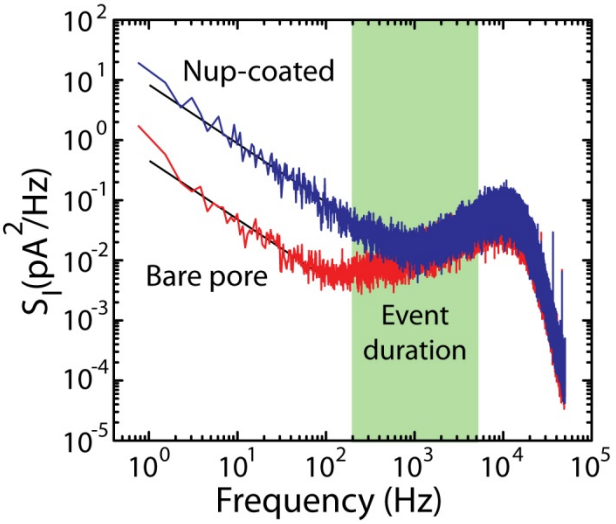

Figure S6. Noise characterizations shows characteristic 1/f-type (black solid lines) low-frequency noise of different magnitude, and a comparable noise level at high-frequencies for both a bare (red) and a Nup98-coated pore (blue). The range in which typical translocation events occur (roughly, 0.2 – 5 ms) is indicated in green.

Additionally we studied the noise in a range of voltages (25-200mV). For the current power spectra S_I (Fig.S7a and Fig.S7b), we find that low-frequency noise increases with the applied voltage, for both bare and Nup98-coated pores, as expected for resistance fluctuations. By contrast, the high-frequency noise is independent of voltage, as expected, because this noise derives from the SiN membrane. The low-frequency noise in the normalized current power spectra (S_I/I^2) is independent of applied voltage for both a bare and a Nup98-coated pore (Fig.S7c), and both display a typical 1/f-type character (Fig.S7d).

© 2011 Macmillan Publishers Limited. All rights reserved.

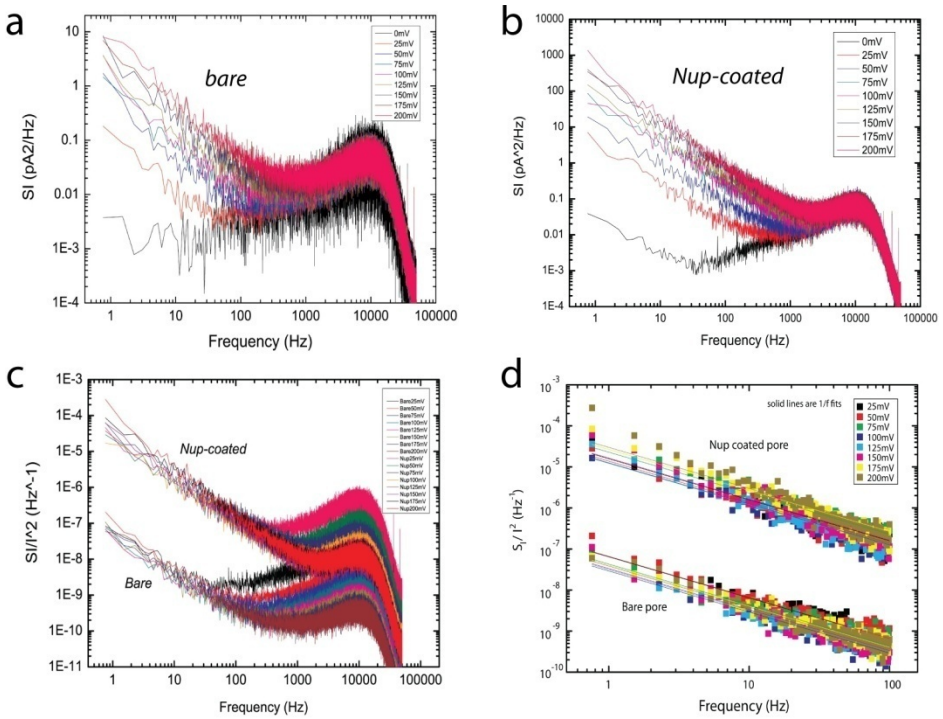

Figure S7. (a) Current power spectral densities of a bare nanopore at a range of voltages (25-200mV). (b) Current power spectral densities of a Nup98-coated nanopore using a similar voltage range. The low-frequency noise increased for all applied voltages, while the high-frequency noise stays constant. (c) Normalized current power spectral density S_I/I^2 for a bare and a Nup98-coated pore for voltages in the range 25-200 mV. (d) Low-frequency normalized current power spectral density S_I/I^2 for a bare and a Nup98-coated pore. In both cases we observe a 1/f-type of dependence for all voltages probed. The solid-lines are fits to $S_I/I^2=A/f$.

7. Alternative exclusion structures

As mentioned in the main text, in our measurements of ionic current what we measure is the "free" conducting volume of the pore and not a particular configuration of Nups in the pore. While there are several good reasons to regard our model 2 with an open channel in the middle of the pore as the natural choice for interpreting the striking data of a cutoff in the conductance versus diameter (Fig.2a), there are different possible geometrical models that can explain our data. Figure S8 shows some possible alternative exclusion structures.

© 2011 Macmillan Publishers Limited. All rights reserved.

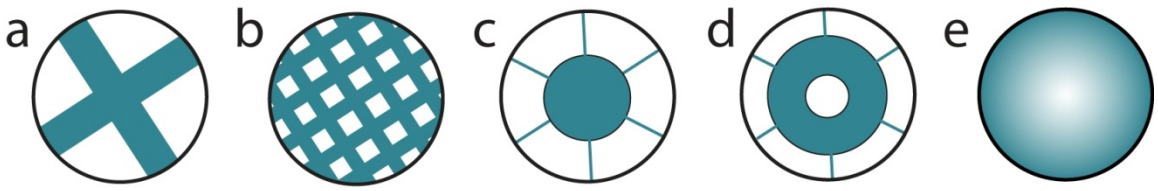

Figure S8. Alternative exclusion structures (representations of the reduction of the pore volume induced by the Nup coating, with dark referring to higher Nup density) to models 1 and 2 presented in Fig.2. Based on the current data, which essentially measures the excluded volume in the pore, it is not possible to discriminate between these more complicated models.

In reality the situation will likely be some subtle mixture of different models, with for example a low density of (likely dynamic) Nups with a certain mesh size in the middle of the pore. This could also explain why BSA transport is inhibited (if the mesh size is approximately smaller than the size of BSA) even though the time-averaged density of Nups in the center of the channel is lower than at the edges.

8. Example events of Impβ translocations through a Nup153-modified pore

Figure S9. Example ion current traces for Impβ translocation through a Nup153-modified pore. The data was filtered at 2 kHz for display purposes.

© 2011 Macmillan Publishers Limited. All rights reserved.

9. Analysis of re-entry events of Impβ

From an analysis of the electrical signals, viz., the times between Impβ events, we can obtain additional evidence that Impβ is indeed translocating and not merely binding at the pore. Events are defined as temporal excursions from the baseline current. Because of the applied electric field, in the bare pore there is no reason to suspect proteins will not translocate through the pore once they entered the pore. However, in the Nup-modified pore, there is a barrier to translocate and hence, in principle, Impβ might bind to the Nup-modified pore and exit at the "wrong" side, namely the entry side instead of the exit. In this case, however, it will be driven back into the pore again by the electric field. This would yield a second event in the current signal that quickly follows the first event, see Fig.S10.

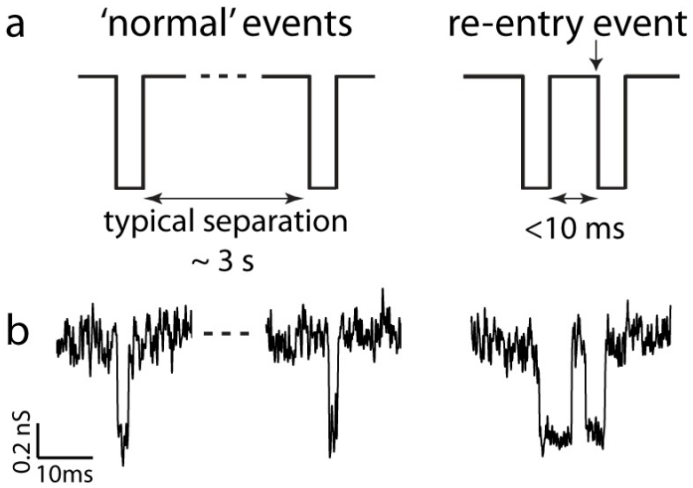

Figure S10. (a) For 'normal' events the typical separation between events is a few seconds. For what we term "re-entry events" (a second current dip rapidly following a previous current dip), the time separation is very short (<10 ms). (b) Experimental data (filtered at 2kHz) showing example events corresponding to the cartoon in a.

Remarkably, for Nup-coated pores, we indeed find a clear overrepresentation (see Fig.S11) of such what we term "re-entry events" compared to bare pores: a second current dip following a previous current dip within a few ms (in contrast to the typical event separation which is a few seconds). The occurrence of these events indicates that about 90% of the events signal a normal translocation event, whereas in about 10% of the occasions Impβ proteins exit at the entry side and re-enter the pore, as we discuss in more detail below.

© 2011 Macmillan Publishers Limited. All rights reserved.

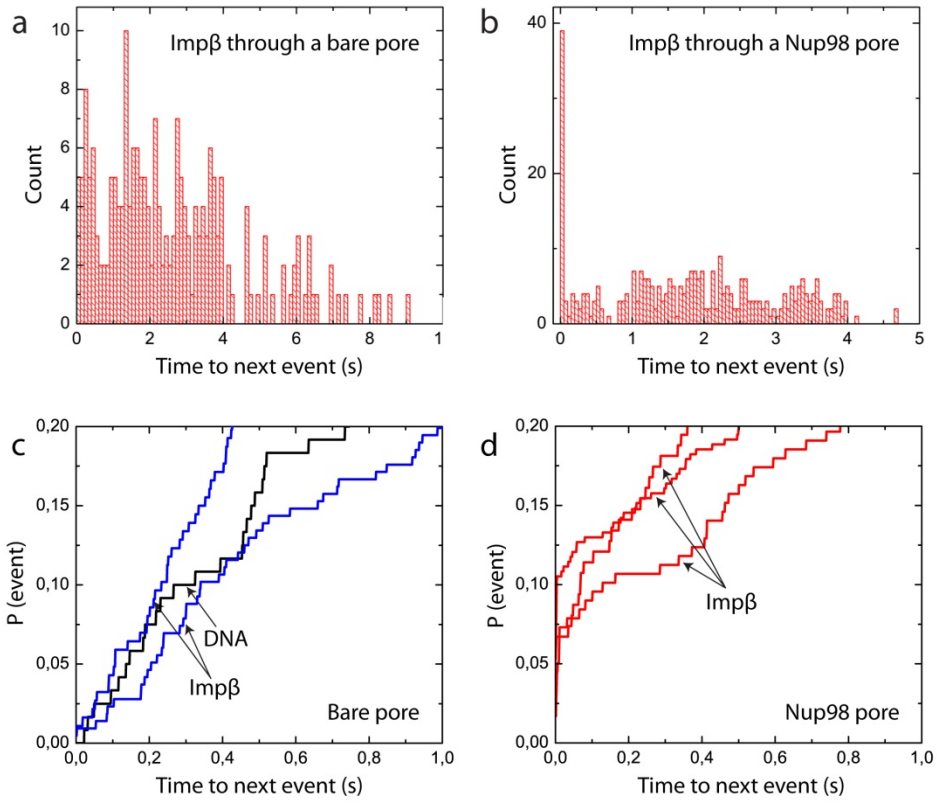

Figure S11. Re-entry analysis. (a,b) Distributions of times between Impβ events in a bare and Nup98-modified pore, respectively. (c,d) Relative fraction, *P*, of events occurring within a time, *t*, after the previous event, in a bare and Nup98-modified pore, respectively. The data extrapolate to P(0)=0 for the bare pore (both for DNA or Impβ translocation), whereas a finite P(0) is obtained for Impβ in Nup-coated pores.

The re-entry process can be modeled quantitatively (A. Y. Grosberg and Y. Rabin, "Correlations between translocation events: possibility of re-entrance", unpublished) which allows to extract the ratio of translocation events versus re-entry events from the times between events. In this model, we assume that diffusively moving particles attempt passing through the pore completely independently from one another. Let us call the refusal probability *p*. We can calculate the probability that no blockage event of any kind happens before time *t* after an initial event as:

$$w(t) = e^{-rt} - p\, e^{-rt}\, (R_{access}/R_{total})\, [1 - (2/d)\cdot(\tau/t)^{d/2}/\,\Gamma(d/2)]\,,$$

with $\tau = a^2/D$ (where *a* is the pore radius and *D* the diffusion coefficient), *d*, the number of dimensions, R_{access} the access resistance to the pore from infinity, and R_{total} the total resistance across the pore including the access resistance. Note that $w(0)$ equals $1 - P(t)$ in the limit for $t \rightarrow$

© 2011 Macmillan Publishers Limited. All rights reserved.

0, with $P(t)$ the relative fraction of events occurring within time t after the previous event, as plotted in Fig.S11. The second term in square brackets becomes negligible because in practice always $t >> \tau \sim 10$ µs. For a 40 nm pore, the access resistance is roughly equal to the pore resistance, hence the expression simplifies to:

$$w(t) = e^{-rt}(1 - p/2).$$

Experimentally, we measure $w(0) = 0.93 \pm 0.02$ for Impβ translocation through a Nup98-modified pore (Fig.S11d). This gives a value of $p = 0.14 \pm 0.04$ for the refusal probability. Note that in the case of a bare pore there is simply no barrier for entry since the hole is essentially an open space that is much larger than the size of a protein. The theory thus predicts a negligible amount of re-entry events for such bare pores. This is consistent with our measurements. (Fig.S11c) where for bare pores we measure $w(0) = 1$, and hence $p = 0$.

10. Overview of measured event amplitudes, translocation times, and event rates

AMPLITUDE ΔG (nS)	BSA	Impβ
bare pore	0.47±0.19	0.59±0.12
Nup98-coated pore	-	0.56±0.12
Nup153-coated pore	0.46±0.08	0.50±0.10

TIME τ (ms)	BSA	Impβ
bare pore	0.17±0.07	0.19±0.04
Nup98-coated pore	-	2.7±0.3
Nup153-coated pore	2.5±0.3	2.2±0.3

EVENT RATE (s^{-1})	BSA	Impβ
bare pore	0.21±0.02	0.27±0.02
Nup98-coated pore	0.0035±0.003	0.21±0.01
Nup153-coated pore	0.05±0.01	0.25±0.02

Table T2. Overview of measured event amplitudes, translocation times, and event rates at 50 mV through pores of 46 nm (Nup98) and 42 nm (Nup153) in diameter. The concentrations used are: [BSA] = 4.2 µM; [Impβ] = 2.9 µM. The measured rates for BSA are rescaled by a factor of 29/42 to accommodate for this difference in concentrations.

© 2011 Macmillan Publishers Limited. All rights reserved.

11. Dwell time histograms on linear scale

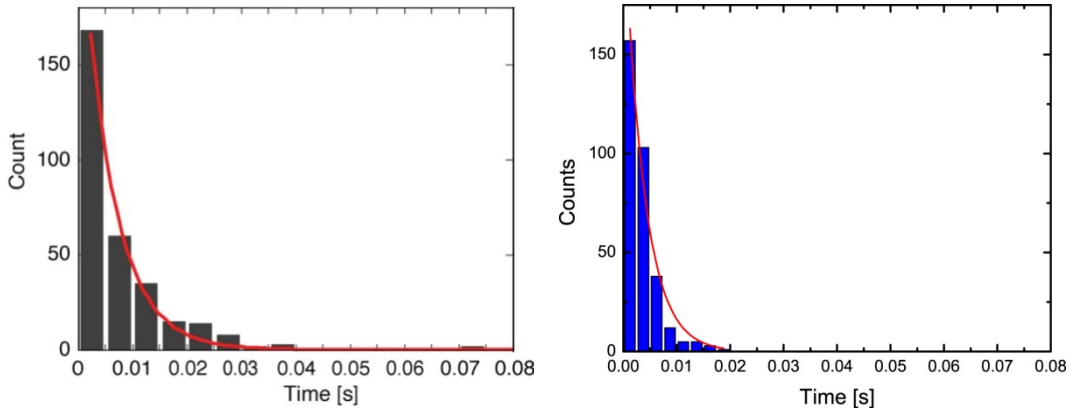

Figure S12. Comparison of the exponential distributions of dwell times. Left: data from Ref. 3 on permeabilized cells, with an exponential decay time constant of 5.8 ± 0.2 ms. Right: our data on biomimetic NPCs, the exponential fit gives $\tau = 3.8 \pm 0.2$ ms.

12. Event frequency versus voltage

It is useful to comment once more on the role of the applied electric field in our experiments. We find the event rate for Impβ to be exponentially dependent on the applied voltage (Fig.S13). This indicates[4] that the delivery of new Impβ proteins to the pore entrance occurs through electrophoretic transport from bulk solution, rather than, for example, by lateral diffusion along the top membrane. Furthermore, during the time that the Impβ interacts with the Nups in the pore, the field exerts a small electrophoretic force (likely of order a few pN) to the Impβ protein which biases it toward the pore exit, thus favoring the protein to leave the exit into the *trans* chamber rather than to return to the *cis* chamber. Such a directional bias has also been suggested for NPCs in vivo, for example due to an affinity gradient along the NPC channel[5] or simply by the ratcheting effect of the RanGTP unloading of Impβ from the nuclear side of the NPC[6].

© 2011 Macmillan Publishers Limited. All rights reserved.

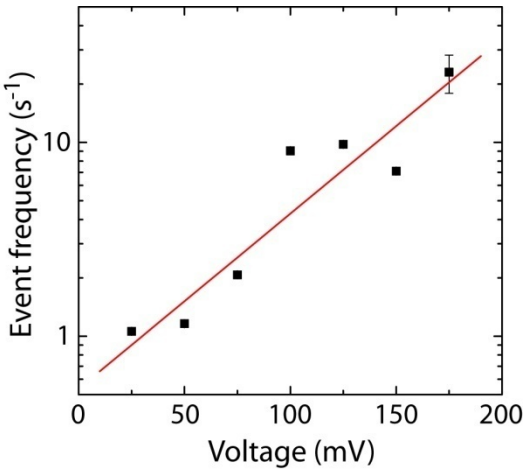

Figure S13. We find that the event rate Γ for Impβ translocations through a Nup98-coated pore increases exponentially with voltage. We fit an exponential function $\ln \Gamma = c_1 + c_2 V$ to the data as shown by the red line, yielding $c_2 = 0.009 \pm 0.002$ mV^{-1}. Impβ concentration used for this data set was 4.5 μM; pore diameter was 35 nm.

13. Nanopore array

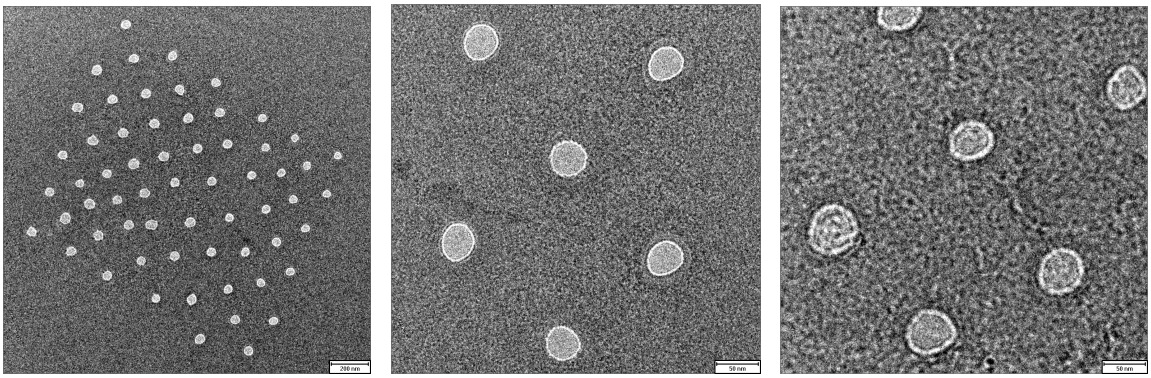

Figure S14. TEM image of nanopore array (left and middle) before coating and (right) after coating. The array consists of 61 nanopores with diameters of 43 ± 3 nm. The measured ionic conductance was stable over time, and decreased from 1840 nS before coating to 257 nS after coating, as expected from Fig.2.

© 2011 Macmillan Publishers Limited. All rights reserved.

14. TIRF

To rigorously prove that the Impβ proteins have translocated is a challenging effort because the amount of protein that is translocated to the *trans* chamber is very small (low attomolar) and no PCR analogue exists for proteins. Nonetheless, we have performed experiments where we optically imaged the proteins that translocated to the *trans* chamber. Specifically, we have labeled Impβ with a fluorescent dye (Alexa488) and collected all the proteins that translocated to the *trans* chamber after a measurement to subsequently visualize these translocated proteins. The collected material was deposited on a microscope glass cover slip and imaged using TIRF. Because the expected number of molecules in the *trans* chamber is very small in a typical experiment, we made an array of nanopores consisting of 61 Nup-98 coated nanopores of 43 ± 3 nm in diameter (Fig.5a) and ran the experiment overnight to maximize the number of molecules in the *trans* chamber. Fig.S15 shows a dilution series, as well as the material collected from the *trans* chamber. The signal is clearly above background.

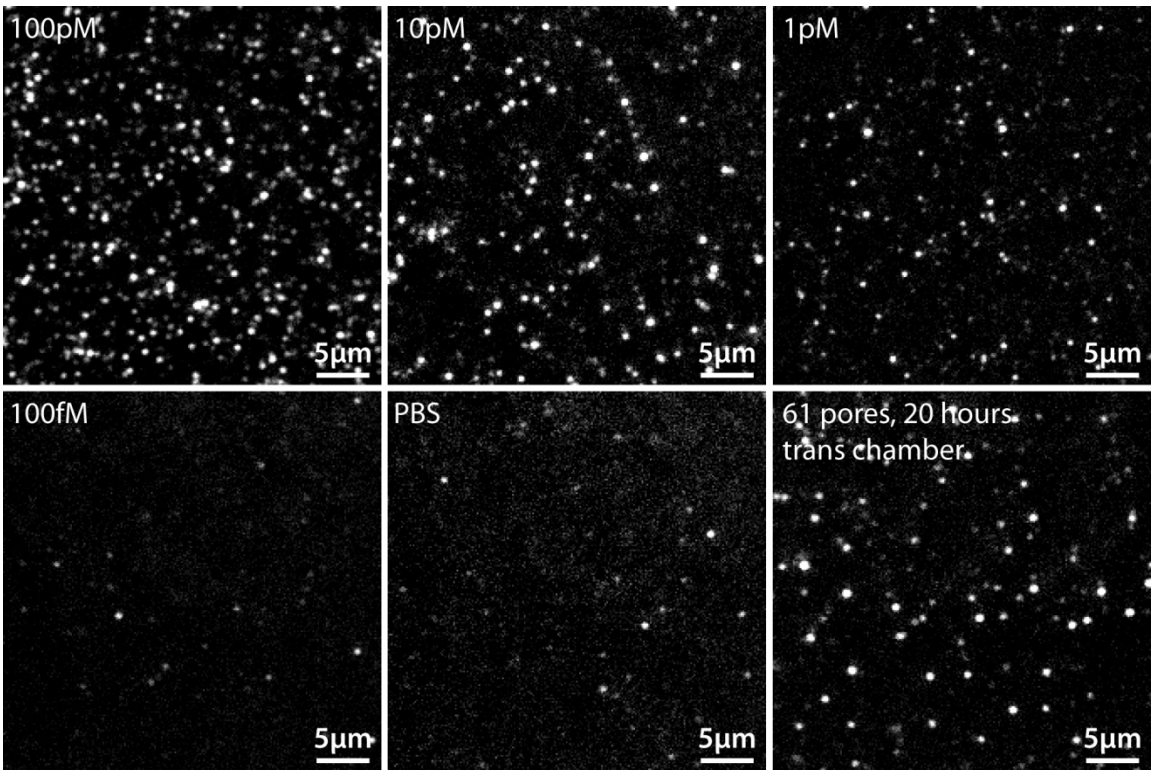

Figure S15. TIRF data. Dilution series of Impβ-Alexa488 (100pM, 10pM, 1pM, 100fM), buffer only (PBS), and the contents of the experimental result with Impβ-Alexa488 from the *trans* chamber (see manuscript).

© 2011 Macmillan Publishers Limited. All rights reserved.

Fig.S16 shows the results of the analysis of the integrated intensity for the two arrays, a buffer only control where buffer was taken out of the flow cell, and a dilution series. The predicted concentration in the *trans* chamber of the array (total volume 20 µL) after 20 hours (for array2; 15 hours for array1) at 100 mV applied voltage with an Impβ concentration of 13 µM in the *cis* chamber is given by: $c_{trans} \approx 61 \cdot (1/s \cdot 13\mu M/3\mu M) \cdot (20 \cdot 60 \cdot 60s)/(6 \cdot 10^{23} \cdot 2 \cdot 10^{-5}\ M^{-1}) = 2$ pM, in good agreement with the TIRF data.

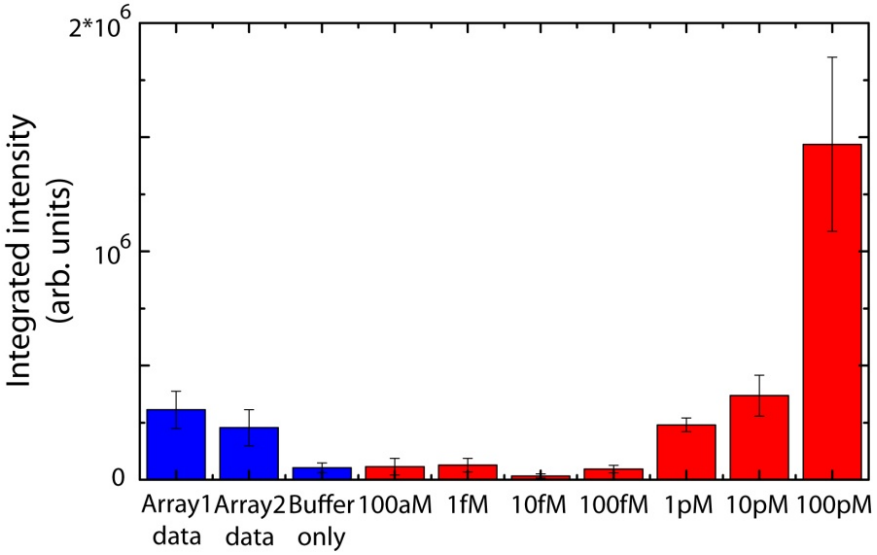

Figure S16. Analysis of the integrated intensity in the TIRF images, including a number of controls (buffer only and a dilution series). See also Materials and Methods in the manuscript.

15. SPR measurements

Traditionally, measurements on NPCs are performed at pH 7.2. Our measurements were done at pH 8.0. To evaluate how this might affect Impß binding interactions, we performed additional surface plasmon resonance (SPR) measurements at both pH 8.0 (Tris) and pH 7.2 (PBS) to compare the binding between Impβ and Nup153 at these two conditions (see Fig.S17). The equilibrium K_D constants are evaluated using the Langmuir isotherm, which shows that Impβ binding at pH 8 that is only slightly weaker than at pH 7.2, giving 431 nM and 387 nM, respectively. This shows conclusively that the slight change in pH does not have a large influence on the binding affinities.

© 2011 Macmillan Publishers Limited. All rights reserved.

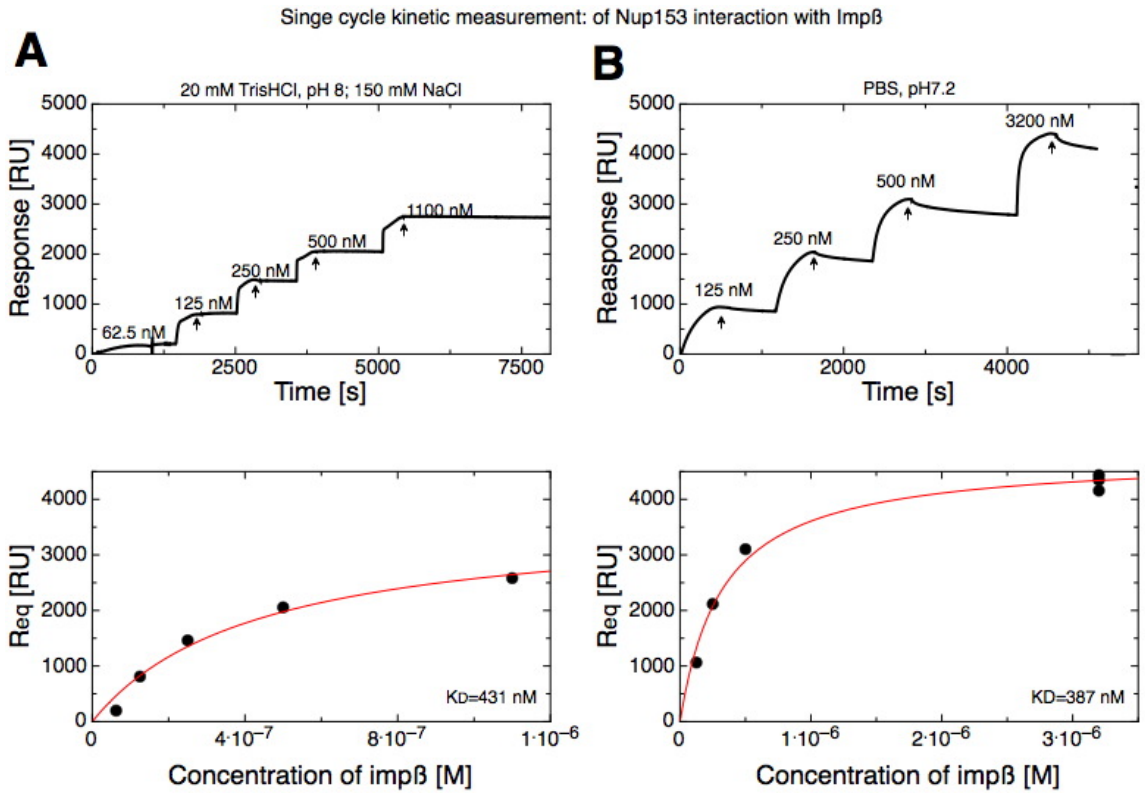

Figure S17. SPR sensograms for Impβ binding to the FG-domain (874-1475) of Nup153 at increasing concentrations (62.5 / 125 / 250 / 500 / 1100 or 3200 nM) in 20 mM TrisHCl, pH 8 buffer with 150 mM NaCl (top, A) and in PBS, pH 7.2 buffer (Invitrogen) (top, B). The arrows (top, A and B) signify to the end of Impβ binding followed by dissociation (rinsing with buffer). The binding responses at steady state (R_{eq}) are obtained by fitting the association parts of the sensogram obtained at each respective Impβ concentration to the equation: $R_t = R_{eq}(1 - e^{-k_{obs}(t-t_0)})$ (not shown), where k_{obs} is an observed rate constant and R_t is a binding response at time t. Then R_{eq} (black points) is plotted versus the corresponding Impβ concentration at pH=8 (A lower panel) and pH=7.2 (B lower panel). Each red line shows a best fit with a Langmuir absorption isotherm

$$R_{eq} = \frac{R_{\max} \times C_{imp\beta}}{C_{imp\beta} + K_D},$$

where R_{max} is a maximal binding capacity and $C_{impß}$ is a concentration of impß. The obtained equilibrium constants are as follows: K_D = 431 nM and K_D = 387 nM for pH8 and pH7.2, respectively.

© 2011 Macmillan Publishers Limited. All rights reserved.

16. Conformational characteristics of Nup98 and Nup153

Protein (total # of aa)	aa range:	Charged/ Hydrophobic	% of length	Conformation
Nup98 (498 aa) (FG-domain: 1-498)	1-160	0.081	32	cohesive
	161-226	1.066	13	repulsive
	227-498	0.117	55	cohesive
Nup153 (602 aa) (FG-domain: 874-1475)	874-1270	0.681	66	repulsive
	1270-1475	0.005	34	cohesive

Table T3. Conformational characteristics of human Nup98 and Nup153 based on charge to hydrophobic ratio (in accordance with Ref. 7).

References

1. Denning, D.P., Patel, S.S., Uversky, V., Fink, A.L., and Rexach, M.. Disorder in the nuclear pore complex: The FG repeat regions of nucleoporins are natively unfolded. *Proc. Natl. Acad. Sci. USA.* **100**, 2450-2455 (2003).

2. Malamud, D. and Drysdale, J.W., Isoelectric points of proteins: A table. *Anal. Biochem*. **86**, 620 (1978).

3. Kubitscheck, U. *et al.* Nuclear transport of single molecules: dwell times at the nuclear pore complex. *J. Cell Biol*. **168**, 233-243 (2005).

4. Smeets, R.M.M. *et al.* Translocation of RecA-coated double-stranded DNA through solid-state nanopores. *Nano Lett*. **9**, 3089-3095 (2009).

5. Ben-Efraim, I. and Gerace, L. Gradient of increasing affinity of importin beta for nucleoporins along the pathway of nuclear import. *J. Cell Biol*. **152**, 411-417 (2001).

6. Stewart, M. Molecular mechanism of the nuclear protein import cycle. *Nature Rev. Mol. Cell Biol*. **8**, 195-208 (2007).

7. Yamada, J. *et al.* A Bimodal Distribution of Two Distinct Categories of Intrinsically Disordered Structures with Separate Functions in FG Nucleoporins. *Mol. Cell. Proteomics*. **9**, 2205 (2010).

© 2011 Macmillan Publishers Limited. All rights reserved.